10-25-2011

Effect of the Deepening of the Tasman Gateway on the Global Ocean

Willem P. Sijp
University of New South Wales

Matthew H. England
Purdue University

Matthew Huber
Purdue University, mhuber@purdue.edu

Effect of the deepening of the Tasman Gateway on the global ocean

Willem P. Sijp,[1] Matthew H. England,[2] and Matthew Huber[2]

Received 18 March 2011; revised 12 July 2011; accepted 21 July 2011; published 25 October 2011.

[1] We examine the effect of the deepening of the Tasman Seaway at the end of the Eocene in a climate model with realistic late Eocene bathymetry and winds. For this, we have constructed an Eocene numerical model based on the University of Victoria climate model with wind forcing derived from a fully coupled Eocene simulation. The model climate state is characterized by an oceanic meridional overturning circulation (MOC) involving Southern Hemisphere sinking and a northward atmospheric moisture transport across the equator. The deepening of the Tasman Seaway in the presence of an open Drake Passage and the associated establishment of the Antarctic Circumpolar Current (ACC) have a limited climatic impact on Antarctica. Nonetheless, the Antarctic deep sinking regions cool sufficiently to lead to a global deep ocean cooling of 3°C. No initiation of Northern Component Water is found, indicating that this may require the development of a more mature ACC. Previous studies suggest that the Ross Sea gyre cools the east coast of Australia, and expected the deepening of the Tasman Seaway to lead to a warming east of Australia due to the introduction of warmer water from the Australo-Antarctic Gulf. We here find that this warming is limited to close to the Australian coast, and that widespread cooling prevails further off shore.

Citation: Sijp, W. P., M. H. England, and M. Huber (2011), Effect of the deepening of the Tasman Gateway on the global ocean, *Paleoceanography*, *26*, PA4207, doi:10.1029/2011PA002143.

1. Introduction

[2] The past 50 million years have witnessed a long term cooling trend culminating in the present climate marked by bipolar glaciation and "ice ages." The Eocene-Oligocene Transition reflects one of the most profound climatic reorganizations of this period, which culminated in the oxygen isotope event Oi-1 ca. 33.55 Ma, the major earliest Oligocene $\delta^{18}O$ increase [see *Miller et al.*, 1987; *Zachos et al.*, 2001; *Zachos and Kump*, 2005; *Miller et al.*, 2009]. Large Antarctic ice sheets are thought to originate at this point [*Miller et al.*, 1991; *Zachos et al.*, 1996] and became more permanently established at the middle Miocene (ca. 14.8 Ma [see *Miller et al.*, 2009]). These shifts in Cenozoic climate were set against a background of a general long-term trend of declining atmospheric CO_2 [*Pagani et al.*, 2005; *Pearson et al.*, 2009]. The late Pliocene (ca. 2.6 Ma) saw northern hemisphere ice volume increase [*Shackleton et al.*, 1984].

[3] The transition to a glaciated climate state was completed in distinct steps, with an increasing influence of ice volume on the oxygen isotope record [*Katz et al.*, 2008], and was accompanied by a 1 km deepening of the calcite compensation depth completed within 300 kyr [*Coxall et al.*, 2005]. Climate cooling is global [*Liu et al.*, 2009; *Lear et al.*, 2008]. Terrestrial ice modeling work suggests that the northern hemisphere remained largely ice free [*DeConto et al.*, 2008]. This climatic turning point at the end of the Eocene and the deepening of the Tasman Seaway appear coeval, leading *Kennett* [1977] and *Berggren and Hollister* [1977] to hypothesize a causal relationship. In this view, the oceanic thermal isolation arising from the development of the Antarctic Circumpolar Current (ACC) leads to cool Antarctic conditions favorable for the emergence of permanent large-scale terrestrial glaciation.

[4] *Stickley et al.* [2004] find that the deepening of the Tasman Seaway occurred about 2 million years before the onset of Antarctic glaciation. The length of this time lag would preclude a direct causal relationship. However, the timing of the development of an eastward flow strong enough for a thermal isolation effect within that time frame is unclear. The lack of cooling at ODP Site 1172 (east Tasman Plateau) across the Eocene/Oligocene boundary found by *Stickley et al.* [2004] may be a result of the northward location of this site (see *Sijp et al.* [2009] for a discussion). The timing of the deepening of Drake Passage (DP), the seaway between Antarctica and South America, is less well constrained to between 20 and 40 million years ago [*Barker and Burrell*, 1977; *Lawver and Gahagan*, 1998; *Scher and Martin*, 2006], but recent timing estimates by *Livermore et al.* [2005] led these authors to argue that the deepening of DP may have constituted a trigger for Antarctic glaciation. In short, the effect of ocean gateways on

[1]Climate Change Research Centre, University of New South Wales, Sydney, New South Wales, Australia.
[2]Department of Earth and Atmospheric Sciences, Purdue Climate Change Research Center, Purdue University, West Lafayette, Indiana, USA.

0883-8305/11/2011PA002143

Antarctic glaciation remains unclear also from the point of view of timing.

[5] Numerical model studies have attempted to assess the oceanic thermal isolation of Antarctica by applying a small land bridge between Antarctica and South America in present-day [*Mikolajewicz et al.*, 1993; *Nong et al.*, 2000; *Sijp and England*, 2004, 2005] or idealized [*Toggweiler and Bjornsson*, 2000] model continental configuration, shutting the DP gap. Closure of the DP gap enables meridional oceanic flow with a western land boundary, allowing the development of a zonal pressure gradient and a geostrophic meridional current across the DP latitudes. This can lead to a large Southern Hemisphere (SH) overturning cell when DP is closed, associated with enhanced poleward heat transport across the Southern Ocean [e.g., *Mikolajewicz et al.*, 1993; *Sijp and England*, 2004]. This strong southern sinking is also confirmed within a realistic Eocene bathymetry for present-day CO_2 by *Najjar et al.* [2002], albeit under restoring conditions for salinity. These model results, where an ACC is absent, only yield some Antarctic cooling in response to the deepening of the Drake Passage, lending just moderate support to *Kennett*'s [1977] hypothesis.

[6] In keeping with the results of *Toggweiler and Bjornsson* [2000], *Huber and Sloan* [2001], *Huber and Nof* [2006], and *Huber et al.* [2003, 2004] find enhanced heat transport into the Southern Hemisphere withrespect to present in fully coupled simulations of Eocene climate with shut Tasman gateway configuration, but those studies also found no increase in southward transport poleward of 45°S latitude. Thus those studies concluded that the deepening of any Southern Ocean (SO) gateway is unlikely to have caused Antarctic glaciation by itself, a view is further reinforced by the seminal modeling work of *DeConto and Pollard* [2003]. Instead, decreasing pCO_2 passes a threshold value whereby height-mass balance feedbacks allow the rapid buildup of an Antarctic ice sheet during orbital configurations favoring cool summers. There is debate about the interpretation of the benthic $\delta^{18}O$ record, as the stepwise shifts at the Eocene-Oligocene Transition may reflect both cooling and an increase in terrestrial ice (see *Sijp et al.* [2009] for references). *Liu et al.* [2009] simulate a significant benthic cooling of between 3 and 5°C with concurrent Antarctic glaciation, and also emphasize the role of declining atmospheric pCO_2 in this cooling.

[7] *Tigchelaar et al.* [2010] use an 8-box model to examine an interesting interpretation of the 2-step $\delta^{18}O$ signal at the E-O boundary. Under a gradually decreasing pCO_2 scenario, they force their box model to first exhibit an Meridional Overturning Circulation (MOC) transition from southern sinking to bipolar sinking by applying an artificial fresh water pulse, followed by the inception of Antarctic ice in their southern box. The MOC switch in their model leads to a 2.3°C cooling of their deep ocean box and they attribute the first step in the E-O signal to deep ocean cooling associated with a switch in MOC polarity. The second step in the signal is derived mainly from the inception of Antarctic terrestrial ice. However, as will be shown here, this initial deep ocean cooling may also be achieved simply by the deepening of Southern Ocean gateways during this period.

[8] *Sijp et al.* [2009] examine the interplay between ocean gateway changes and atmospheric CO_2 concentration (pCO_2) in determining Antarctic and deep ocean warmth. They find that deep ocean temperature and Antarctic SST cool in response to closing DP in the model, and that the magnitude of this cooling increases with increasing pCO_2. This is mainly due to the reduction in Antarctic sea ice at high levels of pCO_2. However, the lack of bipolar cooling found in this study further re-enforces the primacy of greenhouse gas concentrations along with unknown climatic feedbacks as drivers for global cooling around the Eocene/Oligocene boundary. Nonetheless, the Antarctic climate effects and changes in deep ocean temperatures in response to gateway changes are far from negligible. Furthermore, *Najjar et al.* [2002] find a 2°C cooling when changing from an Eocene bathymetry to that of the modern-day in their present-day CO_2 runs, indicating aspects of the Eocene bathymetry that favor a warmer deep ocean.

[9] This motivates further study of late Eocene gateway effects in order to tease out the contributions of pCO_2 and gateway changes to the cooling of Antarctica and the deep ocean over the Cenozoic. *Sijp et al.* [2009] use a present-day geometry and present-day winds and they examine the Drake Passage impact while the Tasman Seaway remains unchanged. Part of the climatic response to deepening Drake Passage in their model arises from a switch from strong southern sinking to the modern conveyor-belt circulation where deepwater forms in the North Atlantic and overlies Antarctic Bottom Water (AABW), ultimately upwelling in the Southern Ocean or the low-latitude Indian and Pacific. Due to significant differences between the early-Oligocene bathymetry and that of the present day, the early Oligocene overturning circulation almost certainly differed from that of today. For instance, the existence of a Panamanian Seaway likely prevented the development of a strong salinity contrast between the Pacific and the Atlantic [*von der Heydt and Dijkstra*, 2006; *Steph et al.*, 2006], and a narrow width of Southern Ocean gateways allowed a weaker throughflow of the ACC. Indeed, *von der Heydt and Dijkstra* [2006, 2008] find sinking in both the North Pacific and Atlantic in their Oligocene model for this reason.

[10] Here, we use realistic late-Eocene bathymetry and an estimate of late-Eocene wind forcing to argue that the deepening of the Tasman Seaway to 1300 m depth, and the associated establishment of a limited ACC, have an impact on Antarctic climate. In particular, the Antarctic deep sinking regions cool sufficiently to lead to a deep ocean cooling of 3°C. *Huber et al.* [2004] noted that the Ross Sea gyre cools the east coast of Australia, and expected the deepening of the Tasman Seaway to lead to a warming east of Australia due to the introduction of warmer water from the Australo-Antarctic Gulf. We here find that this warming is limited to close to the Australian coast, and that widespread cooling prevails further off shore.

2. The Model and Experimental Design

[11] We use a modified version of the intermediate complexity coupled model described in detail by *Weaver et al.* [2001], the so-called UVic model, with wind forcing estimated from a full coupled climate model including a dynamic atmosphere. The UVic model comprises an ocean general circulation model (GFDL MOM Version 2.2 [*Pacanowski*, 1995]) coupled to a simplified one-layer

Table 1. Description and Definition of Experiments

Experiment	Description	pCO_2 (ppm)
CNTRL	Control case. Tasman Seaway closed; DP open.	1500
TAS_{op} DP_{op}	As in CNTRL, but Tasman Seaway opened to 1300 m depth.	1500
TAS_{op} DP_{cl}	As in CNTRL, but Drake Passage closed and Tasman Seaway opened.	1500
TAS_{cl} DP_{cl}	As in CNTRL, but Drake Passage closed and Tasman Seaway closed.	1500
PD	Present-day simulation with present-day geometry.	280

energy-moisture balance model for the atmosphere and a dynamic-thermodynamic sea-ice model of equal global domain. We have replaced the present-day bathymetry, topography and vegetation with the reconstruction of a late Eocene bathymetry, topography and vegetation used by *Huber et al.* [2004]. The bathymetry is shown in Figure 2 of *Huber et al.* [2003]. The horizontal resolution has been adjusted to 2.4° longitude by 1.8° latitude. The number of vertical levels has been increased from 19 to 40 for our Eocene simulations. Sub-grid scale eddy effects on tracer transport is represented by the parameterizations of *Gent and McWilliams* [1990]. Vertical mixing due to wind and vertical velocity shear is achieved using the turbulent kinetic energy scheme of *Blanke and Delecluse* [1993] based on *Gaspar et al.* [1990]. Although air-sea heat and freshwater fluxes evolve freely in the model, a non-interactive wind field is employed. The wind stress forcing is taken from the Eocene simulations of *Huber and Nof* [2006] to form a seasonal cycle from the monthly fields. No flux corrections are used, allowing surfacetemperature and salinity to vary freely in the model.

[12] The atmospheric radiative balance is fed by solar insolation, where orbital values are fixed at the year 1850. The obliquity is 23.46°, the eccentricity 0.0167 and the longitude of perihelion is 279.47°. The obliquity can be considered close to "average," whereas eccentricity is below average. The point here is that we choose a fixed set of orbital parameters, as our main concern will be the effect of tectonic changes. Atmospheric moisture transport is achieved by way of advection and diffusion using constant moisture diffusivity. Precipitation may fall as snow or rain. Snow cover is limited to a maximum height of 10 m, more than can melt during summer. We have removed the standard specification of the increased surface elevation and albedo associated with ice sheets in Antarctica and Greenland, so that no a-priori assumptions of ice-sheets exist there. Following this procedure, snow heights of 10 m indicate the places were ice sheet inception is likely. No cloud scheme is included, precluding potentially important drivers of high latitude greenhouse warmth [see *Abbot et al.*, 2009]. More detailed descriptions of the model are given by *Sijp et al.* [2006, 2009].

[13] We conduct 4 Eocene experiments where atmospheric pCO_2 is set to 1500 ppm, and one present-day experiment where pCO_2 is fixed at 280 ppm. The 1500 ppm value is chosen to create a warm climate, and is on the high end of estimates by *Pearson et al.* [2009] for the late Eocene. Model experiment names and descriptions are given in Table 1. The standard Eocene control run CNTRL employs the wind field and bathymetry of *Huber et al.* [2004], where the Drake Passage has a shallow depth of 1100 m and the Tasman Seaway is closed. Although very shallow throughflow may have occurred throughout the Eocene [see *Stickley et al.*, 2004], transports are unlikely to have been of the magnitude of basin-scale flow and a closed Seaway is therefore appropriate in the setting of a coarse resolution model. A similar procedure was followed by *Huber et al.* [2004]. We will refer to the elimination of the land bridge across the Tasman Seaway in our model as the "deepening" of the Tasman Seaway. The Tasman Seaway is open to mid-depth flow in experiment TAS_{op} DP_{op}. The Drake Passage and Tasman Seaway are shut by a land bridge in TAS_{cl} DP_{cl}, while the Tasman Seaway is opened while the Drake Passage remains shut in TAS_{op} DP_{op}DP. We refer to the pre-industrial run as present-day to indicate its present day bathymetry and wind forcing, although this name is not entirely precise as the present day climate is changing due to greenhouse gas emissions from the burning of fossil fuel. The CNTRL experiment is close in setup to the 1120 ppm experiment by *Huber and Nof* [2006], where identical winds and geometry are used. The TAS_{op} DP_{cl} experiment is included to examine whether temperature effects of the deepening of the Tasman Seaway can be also obtained when the Drake Passage remains closed.

[14] The Eocene and PD experiments were integrated for 5000 years from idealized initial conditions. As we will see, all Eocene runs lead to Southern Hemisphere sinking states. To examine whether the experiments allow multiple equilibria, we have attempted to induce a northern hemisphere sinking state by applying a temporary salinity flux in the north and compensating fresh water flux in the south. This led to a temporary switch to a northern sinking state. However, this state proved unstable once the anomalous salt flux was terminated, and no multiple equilibria were found in our experiments.

3. Results and Discussion

3.1. Discussion of Eocene CNTRL Simulation Climate

[15] The steady state Eocene-like climate of CNTRL is presented in Figures 1 and 2, and summarized in Table 2. The present-day simulation PD yields a global SST average of 17.6°C and air temperature (SAT, equivalent temperature at sea level) average of 14.0°C, both realistic values (Table 2). The Eocene simulation CNTRL yields a global average SST of 25.9°C, a 8.3°C increase over PD. Global average SAT is increased by 9.8°C over PD. Very fresh conditions of around 10 psu prevail in the Arctic (Figure 1a), in agreement with findings by *Waddell and Moore* [2008] and *Gleason et al.* [2009]. This is due to the polar location of this ocean, placing it in an area of net precipitation while lacking significant seaway connections to the world ocean to replenish salt. The only connection is a shallow seaway connecting the Atlantic and the Arctic. In a forthcoming study we will show that the fresh Arctic conditions are highly dependent on the presence of shallow gateways additional

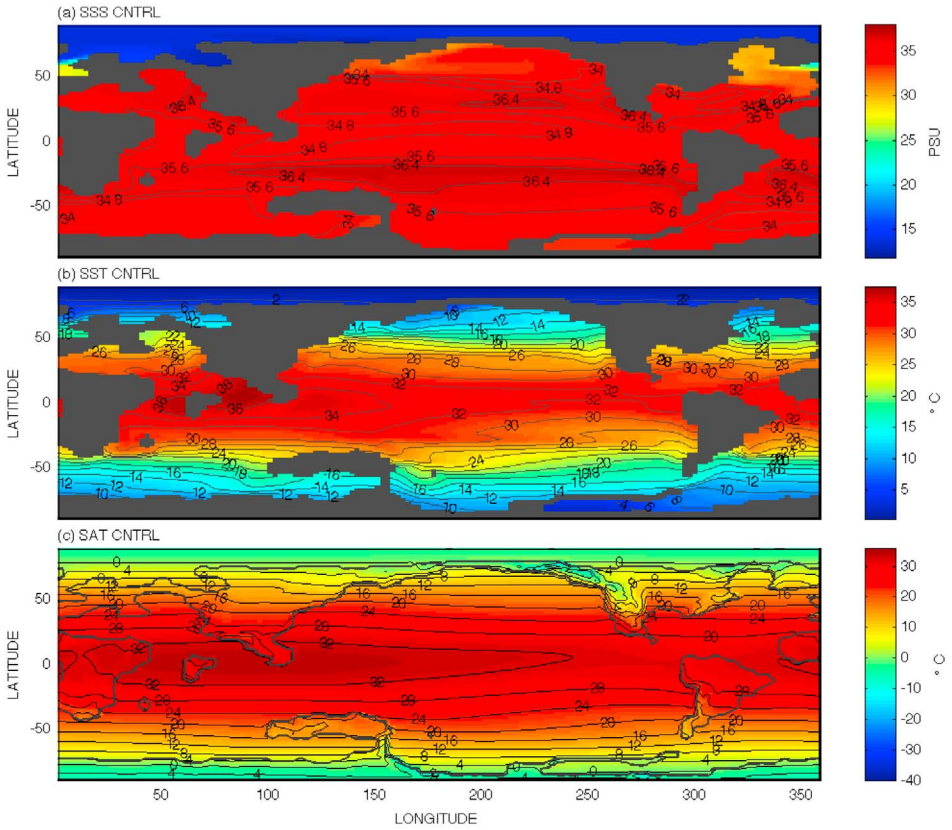

Figure 1. (a) Annual mean sea surface salinity (SSS, in PSU), (b) annual mean sea surface temperature (SST, °C) and (c) annual mean surface air temperature (°C).

to the North Atlantic gateway to the Arctic in our model. Maximum salinity occurs in the subtropical gyres due to net evaporation there. Unlike *Huber et al.* [2003] and *Huber and Nof* [2006], we find no fresher conditions in the Southern Ocean. Mixed layer depths are deepest in the Ross Sea, where bottom water ventilation takes place (Figure 2a). Ventilation to intermediate depth occurs in the North Pacific and around the tip of South America. In agreement with *Huber and Nof* [2006], there is no perennial snow cover in the CNTRL Eocene simulation (Figure 2b), with the exception of very limited high altitude regions. Antarctica receives snow during winter months, but no permanent ice sheet develops as snow melts during summer. Antarctica is free of sea-ice year round (Figure 2b). Sea-ice occurs seasonally in the high latitudes of the Arctic, in agreement with the findings of *Stickley et al.* [2009].

[16] Tropical sea surface temperature (SST) reaches 36°C in the tropical warm pool spanning the eastern Pacific and the Tethys/Indian ocean area east of India, an island in our model (Figure 1b). The tropical temperatures of around 32°C off present-day Tanzania are in reasonable agreement with the reconstructions of *Lear et al.* [2008] in Tanzania and *Liu et al.* [2009] in various tropical and midlatitude regions. Antarctic sea surface temperatures generally remain above 10°C, with the exception of a poorly ventilated region south of the Antarctic Peninsula. The 10–12°C SST contours near the Antarctic coast are in good agreement with the simulations of *Liu et al.* [2009]. In contrast, annually averaged Arctic sea surface temperatures go down to 1–4°C. *Liu et al.* [2009] find 20°C surface temperatures at high latitude ODP/DSDP sites 336 (North Atlantic) and 511 (east of Drake Passage) while our model yields temperatures of 14–16°C there. However, our temperatures at these sites are

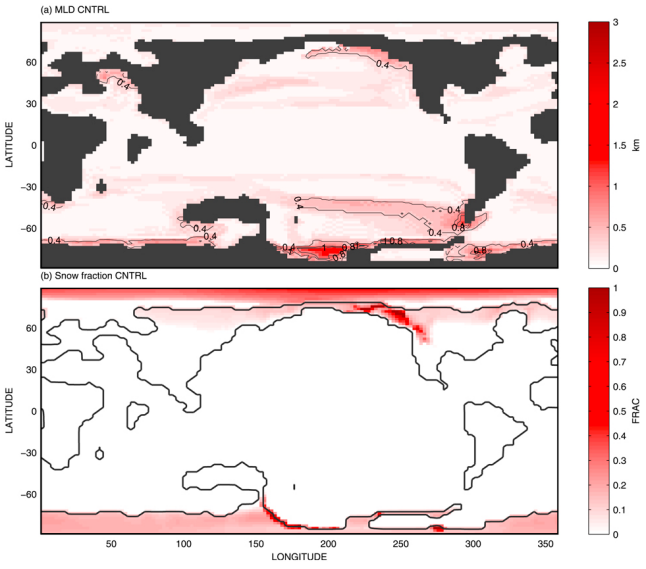

Figure 2. (a) Annual mean mixed layer depth (km) as measured by the vertical mixing scheme and (b) annual snow fraction (fraction 0–1).

Table 2. Key Climate Diagnostics[a]

	CNTRL	TAS_{op} DP_{op}	TAS_{cl} DP_{cl}	TAS_{op} DP_{cl}	PD
Vol. T	10.7	8.6	10.5	10	3.7
SST	25.9	25.9	25.8	25.8	17.7
Deep T	9.2	6.2	8.8	8.3	1.9
SAT	23.8	23.9	23.8	23.8	14.1

[a]Global volume-averaged potential temperature (row 1, labeled "Vol. T"), globally averaged sea surface temperature (row 2, labeled "SST"), averaged deep ocean temperature below 3000 m depth (row 3, labeled "Deep T" and globally averaged surface air temperatures (row 4, labeled "SAT") for the experiments CNTRL (column 1), TAS_{op} DP_{op} (column 2), TAS_{cl} DP_{cl} (column 3), TAS_{op} DP_{cl} (column 4) and the present-day run PD (column 5).

in agreement with the Eocene model results of *Liu et al.* [2009]. The SST at ODP site 1172 examined by *Stickley et al.* [2004] and *Bijl et al.* [2009] near present-day Tasmania is between 14–16°C, whereas studies in this region, e.g., *Bijl et al.* [2009] and *Liu et al.* [2009] find values of about 21°C for the late Eocene, and significantly higher temperatures for earlier Eocene time intervals. This suggests that our model fails to capture the high latitude amplification of global warmth that typified the Eocene.

[17] Surface air temperature (SAT) reaches above 34°C around the warm pool (Figure 1c). Annually averaged Antarctic air temperature is around 8°C at the coast, and only drops below freezing deep in the Antarctic interior at high southern latitudes, where the mean air temperature is below −4°C. In agreement with the COUPLEDx4 result of *Huber and Nof* [2006], Antarctic air temperature reaches above freezing in a 1–2 grid cell fringe around Antarctica. The COUPLEDx4 refers to a fully interactive coupled run with an Eocene bathymetry using the National center for Atmospheric Research's Community Climate System Model (CCSM) [see *Huber et al.*, 2004]. Arctic air temperatures are just below freezing in general agreement with the results of *Eldrett et al.* [2009].

[18] Figure 3 shows that the meridional overturning circulation of each Eocene experiment is characterized by a deep cell originating at the Antarctic sea surface and ventilating the bottom of the world ocean. Figure 2a indicates that this cell involves deep sinking from the Ross Sea. *Sijp and England* [2004] and *Mikolajewicz et al.* [1993] find a similar circulation in their Drake Passage closed case, as do *Najjar et al.* [2002] in their Eocene simulation. The southern polarity of the meridional overturning circulation in our CNTRL experiment is in agreement with the findings of *Corfield and Norris* [1996], *Thomas et al.* [2003], *Thomas* [2004], *Via and Thomas* [2006], and *Coxall and Pearson* [2007] that points to deep ocean ventilation from the south. *Tigchelaar et al.* [2010] also find southern sinking in their 8 box model. *Cramer et al.* [2009] argue that homogeneous deep ocean conditions before the late Eocene arose from deep sinking in both hemispheres. *Huber and Nof* [2006], *Huber et al.* [2003], and *Huber and Sloan* [2001] find their zonal mean meridional overturning circulation dominated by northern hemisphere sinking, although significant vertical mass exchange between the surface and the deep ocean occurs around Antarctica in their model, whereby upwelling largely cancels sinking in the zonal mean. Sinking in our CNTRL case is 21 Sv, and there is wind-driven upwelling around 50° S. This gives the overturning stream function the appearance of two anticlockwise cells (Figure 3a).

[19] Figure 4 shows heat transport and zonally and annually averaged surface temperatures, precipitation (P) and evaporation minus precipitation (E-P) in our Eocene model climates and for reference the present-day model climate (PD). Annually averaged Antarctic SAT goes down to −28°C in the present-day pre-industrial simulation, where the presence of an ice sheet and low atmospheric CO_2 (280 ppm) allows low air temperatures. Note that the elevation corresponding to an ice sheet is prescribed in our PD run, and removed in our Eocene runs. Nonetheless, snow is allowed to accumulate to 10 m, a height likely to survive summer. In contrast, the Eocene experiments yield a zonally averaged SAT profile that remains above −4°C in Antarctica, yielding a significant SAT equator to pole gradient reduction of 20°C. Equatorial SAT reaches around 32° in the zonal mean. Zonally averaged Arctic SAT drops just below freezing in the Eocene experiments, whilst temperatures below −12°C are reached in the present day run. Here, in the northern hemisphere, a more modest SAT gradient reduction of around 4°C is realized. Similarly, zonally averaged Antarctic SST reaches down to 10–11°C in CNTRL and 8°C in TAS_{op} DP_{op}, while the present-day model exhibits freezing temperatures at high southern latitudes.

[20] The cool Arctic conditions between 2°C (highest latitudes) and 8°C (towards subpolar regions) are low compared to the temperatures shown by *Bijl et al.* [2009], and arise from the high degree of isolation arising in the absence of oceanic gateways there. A lack of cloud feedbacks may also contribute, as high latitude atmospheric convection may be an important driver of high latitude greenhouse warmth [*Abbot et al.*, 2009]. Overall, a reduction in meridional Eocene SST gradient is more apparent in the southern hemisphere than in the north, and SAT and SST are higher in the Eocene experiments than in the present day experiment at all latitudes due to elevated levels of CO_2. This may be related to the latitudinal asymmetry in oceanic poleward heat transport ((PHT) Figure 4c) where, unlike the PD case, PHT in the Southern Hemisphere (up to over 2 PW) is twice as large as in the Northern Hemisphere (up to less than 1 PW). In contrast, *Huber and Nof* [2006] find a slightly larger PHT in the Northern Hemisphere (up to around 1.5 PW) than in the Southern Hemisphere (up to less than 1 PW). We attribute the asymmetry in PHT in our model to the Southern Hemisphere sinking cell and the absence of Northern Hemisphere sinking. In contrast to our results, the model of *Huber and Nof* [2006] exhibits Northern sinking, leading to a more symmetrical oceanic PHT distribution.

[21] Our Eocene heat transport pattern is similar to that found by *Sijp and England* [2004] and *Sijp et al.* [2009] and is explained further therein. Due to a reduced efficiency of the southern sinking cell, the TAS_{op} DP_{op} experiment exhibits a heat transport of up to 0.7 PW (at southern mid latitudes) smaller in the Southern Hemisphere than CNTRL, while northern Hemisphere heat transport remains more similar. This results in the warmer conditions at high southern latitudes in CNTRL compared to TAS_{op} DP_{op}. Atmospheric heat transport is very similar for all experiments, whereby differences act to compensate the differences in oceanic heat transport (Figure 4d). This can be seen

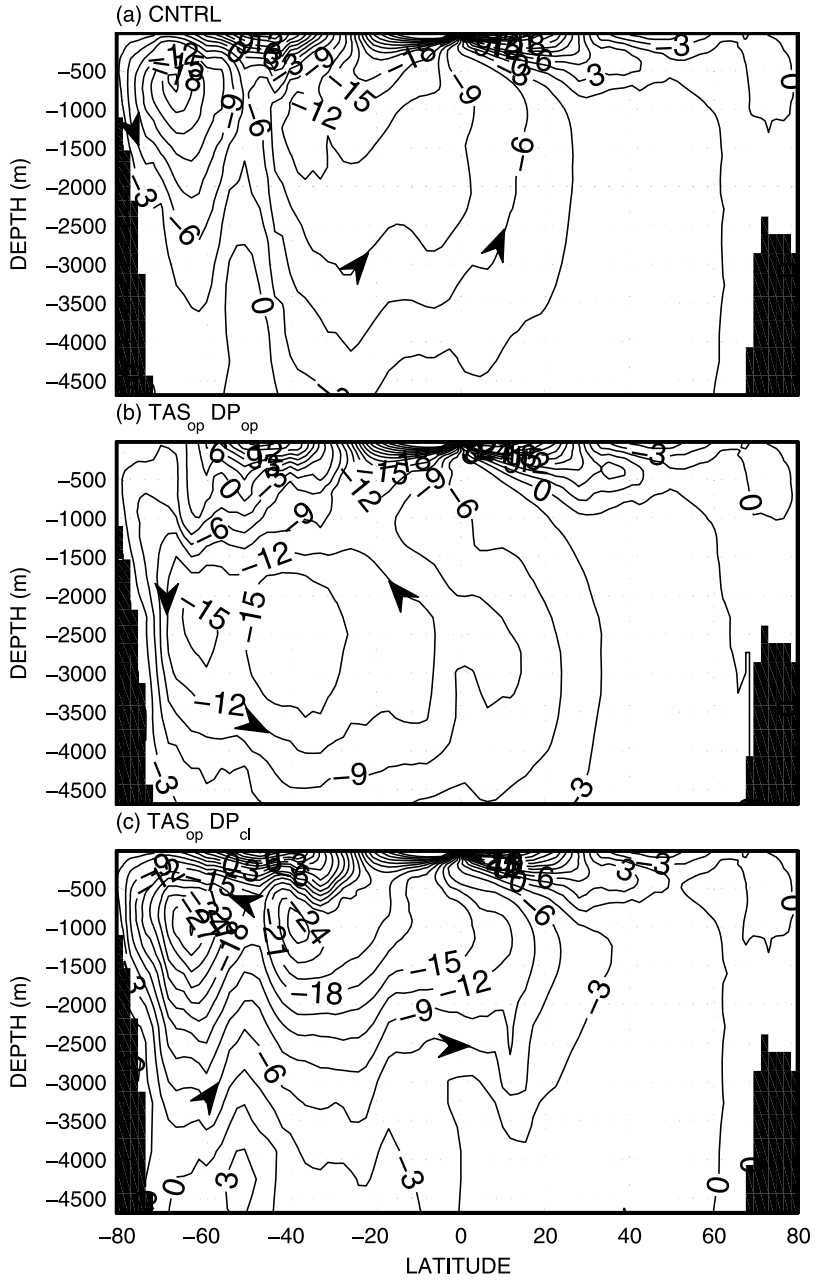

Figure 3. Global meridional overturning circulation for (a) CNTRL, (b) TAS_{op} DP_{op} and (c) TAS_{op} DP_{cl}. To avoid confusion, note that there is no ACC in the experiment shown in Figure 3c, as Drake Passage is closed here. Values are given in Sv (1 Sv = 10^6 m^3 sec^{-1}).

more clearly from the close approximation in magnitude of the atmospheric heat transport difference to the oceanic heat transport difference (Figure 4c).

[22] The Eocene hydrological cycle is significantly enhanced with respect to the present-day (Figures 4e and 4f), as shown by the higher amplitude of ocean FW flux (mainly driven by evaporation - precipitation, E-P) gradients (Figure 4f). Tropical precipitation (P) is increased in the Eocene runs with respect to present-day (Figure 4e). The increase in polar and sub-polar precipitation of TAS_{op} DP_{op} and CNTRL with respect to PD is particularly significant, as it represents an increase from very small values and entails an enhanced latent heat transport to these regions (figure not shown). The FW flux in our model is qualitatively quite similar to that of *Huber et al.* [2004] shown in blue, although our FW flux is of somewhat lower amplitude. Furthermore, there is more precipitation in the Southern Ocean in their model, leading to a suppression of southern sinking. Our model simulates a FW spike in the North Atlantic, likely related to sea ice melt, that may be responsible to reduced northern sinking in our model. This could explain why our simulation exhibits significant southern sinking, whereas the model of *Huber et al.* [2004] exhibits northern sinking and no net southern sinking in the zonal total. An asymmetric hydrological cycle can induce a particular polarity of the global overturning circulation [*Sijp*

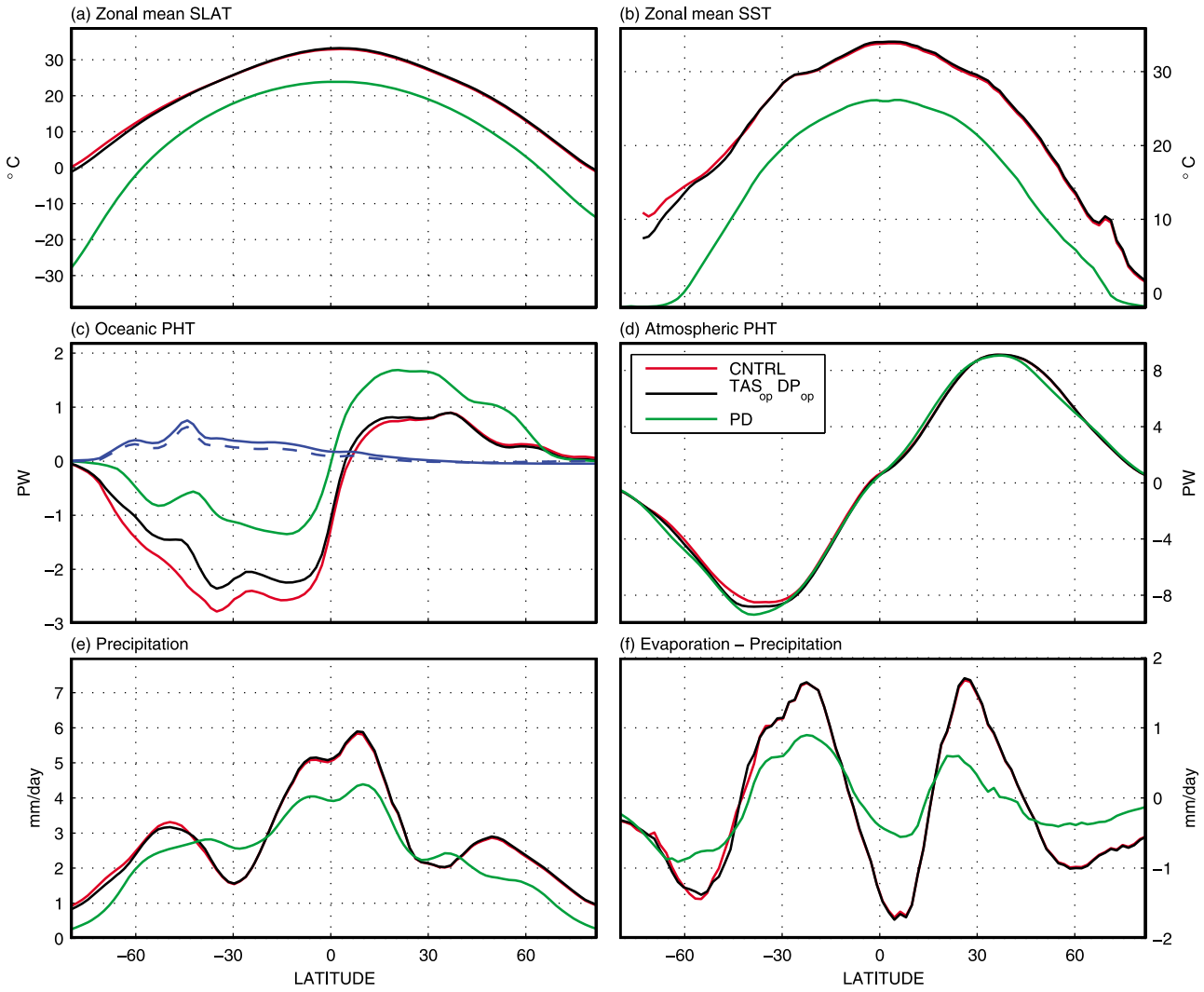

Figure 4. Zonal mean of (a) sea level air temperature (SAT, °C) and (b) sea surface temperature (SST). Total heat transport in (c) ocean and (d) atmosphere, (e) precipitation (mm/day) and (f) surface ocean fresh water (FW) flux (mm/day) for CNTRL (red), TAS_{op} DP_{op} (black) and a present-day simulation (green) and the values of *Huber et al.* [2004] (blue). The difference in ocean (solid) and atmosphere (dashed, multiplied by −1 for easy comparison) heat transport TAS_{op} DP_{op}-CNTRL is shown in blue (Figure 4c).

and England, 2009], offering a potential explanation for the southern sinking in our Eocene model. The Southern Hemisphere overturning cell reinforces the saline conditions by bringing saline subtropical water to the Southern Ocean. In contrast, the absence of a net global meridional overturning southern sinking cell given in the work by *Huber and Nof* [2006] (see also *Huber and Sloan* [2001] where a Northern Hemisphere sinking cell dominates) leads to a fresh Southern Ocean there. Our winds and continental geometry are identical to those of *Huber and Nof* [2006], suggesting the difference in atmospheric heat and fresh water transport as a cause of the difference in meridional overturning polarity between the models.

[23] The barotropic stream function for CNTRL shown in Figure 5 is remarkably similar to that of the COUPLEDx4 case of *Huber and Nof* [2006], with a 50 Sv subtropical gyre in the North Pacific, a very wide 50–60 Sv subtropical gyre spanning the South Pacific and Indian ocean, a confined 20–30 Sv subtropical gyre in the South Atlantic and a 40 Sv Ross Sea gyre. Our North Atlantic subtropical gyre is somewhat weaker than that of *Huber and Nof* [2006] which is likely due to the inclusion of anisotropic viscosity in that study. Also, a 10 Sv flow passes from the Atlantic into the Pacific in our experiments but is comparable to the results of *Huber et al.* [2004]. A somewhat convoluted path returns this streamline to the Atlantic via the Tethys. The overall similarity is to be expected on the basis of the identical wind stress forcing and Eocene bathymetry used in the two models. Perhaps more impressively the results are also very comparable to the barotropic stream function produced in the recent study of *Ali and Huber* [2010] with similar boundary conditions but using a newer, very different version of the NCAR CCSM (version 3). The intermodel consistency indicates that these circulations are very robust.

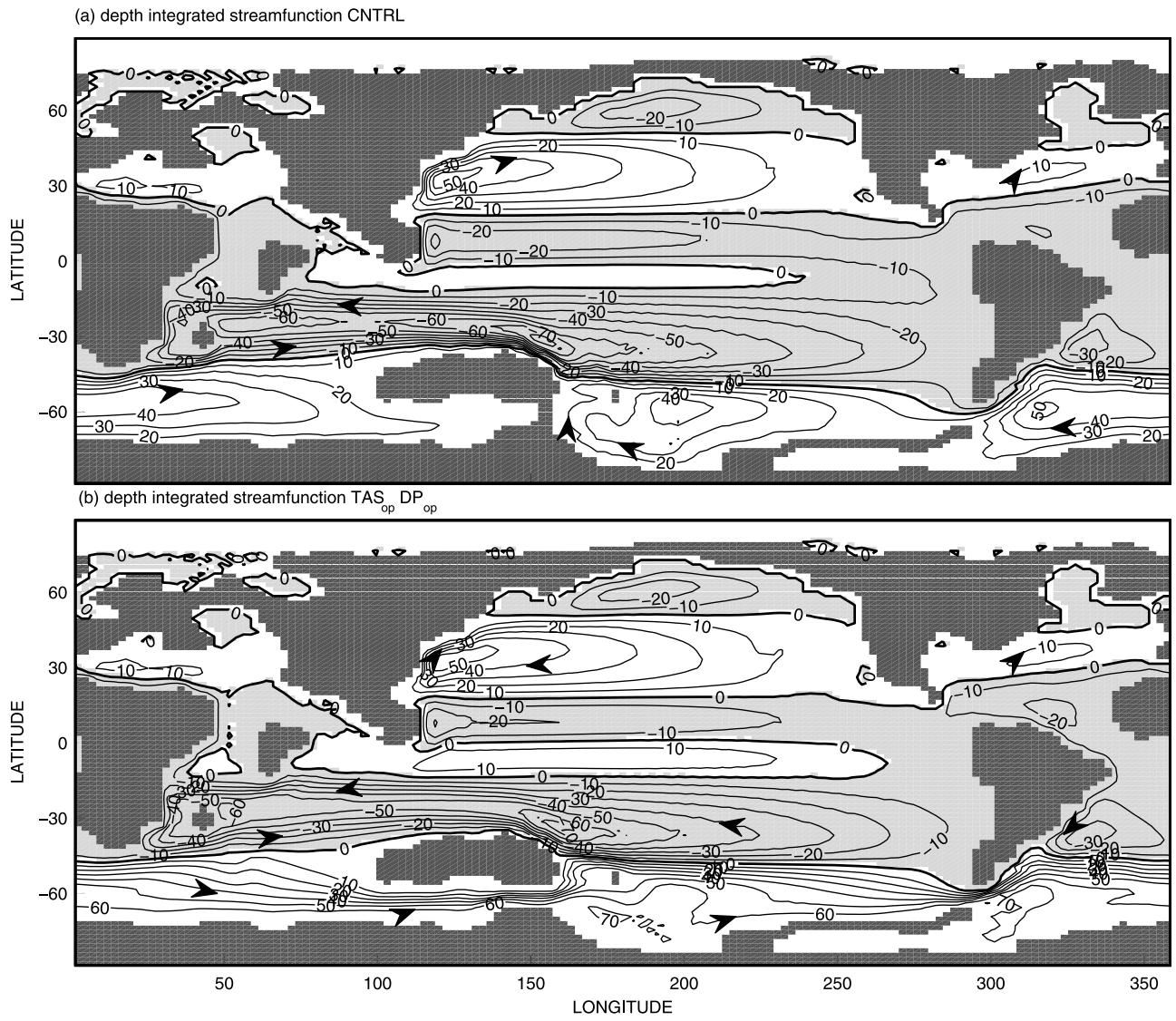

Figure 5. Annual barotropic stream function for (a) CNTRL and (b) TAS_{op} DP_{op}. Values are given in Sv (1 Sv = 10^6 m^3 sec^{-1}).

3.2. Changes Upon the Deepening of the Tasman Seaway

[24] Deepening the Tasman gateway (Figure 3) leads to a reduction in cell strength to around 15 Sv (Figure 3b). However, subtropical water is now required to sink to depths below the sill across the Tasman Gateway (1300 m deep), and net surface flow to the Antarctic sinking regions is obstructed due to the absence of a western boundary [see, e.g., *Toggweiler and Bjornsson*, 2000]. This obstruction leads to a reduction in water participating in the large southern cell circuit [*Sijp and England*, 2005]. *Huber and Nof* [2006] find a reduction of their prescribed SH sinking when detaching Australia from Antarctica in their 1.5 layer idealized model. However, this model does not capture the reduction in meridional flow that is possible across the Tasman Seaway gap latitudes when this gateway is opened. Finally, a closed Drake Passage and open Tasman Seaway leads to a strong southern hemisphere cell of about 27 Sv (Figure 3c), a circulation similar to that of CNTRL but somewhat stronger.

[25] Comparing CNTRL to TAS_{op} DP_{op}, we find similarity in barotropic stream function outside the Southern Ocean for all our Eocene experiments. The southern hemisphere subpolar circulation in CNTRL is divided into a 40 Sv Ross Sea gyre and a 50 Sv subpolar gyre west of Australia and east of Drake Passage (Figure 5a). A 10 Sv circumpolar streamline passes north of Australia. Deepening the Tasman Seaway leads to a 66 Sv circumpolar flow replacing the two subpolar gyres in the southern hemisphere (Figure 5b). As expected, this establishment of the ACC only occurs when the Drake Passage is also open, and the two southern hemisphere subpolar gyres remain intact when the Tasman Seaway is opened while the Drake Passage remains closed (figure not shown). In this case, the Ross Sea gyre is particularly robust with respect to the deepening of the Tasman Seaway, although a 10 Sv streamline now indicates flow from the Indian to the Pacific Ocean via the

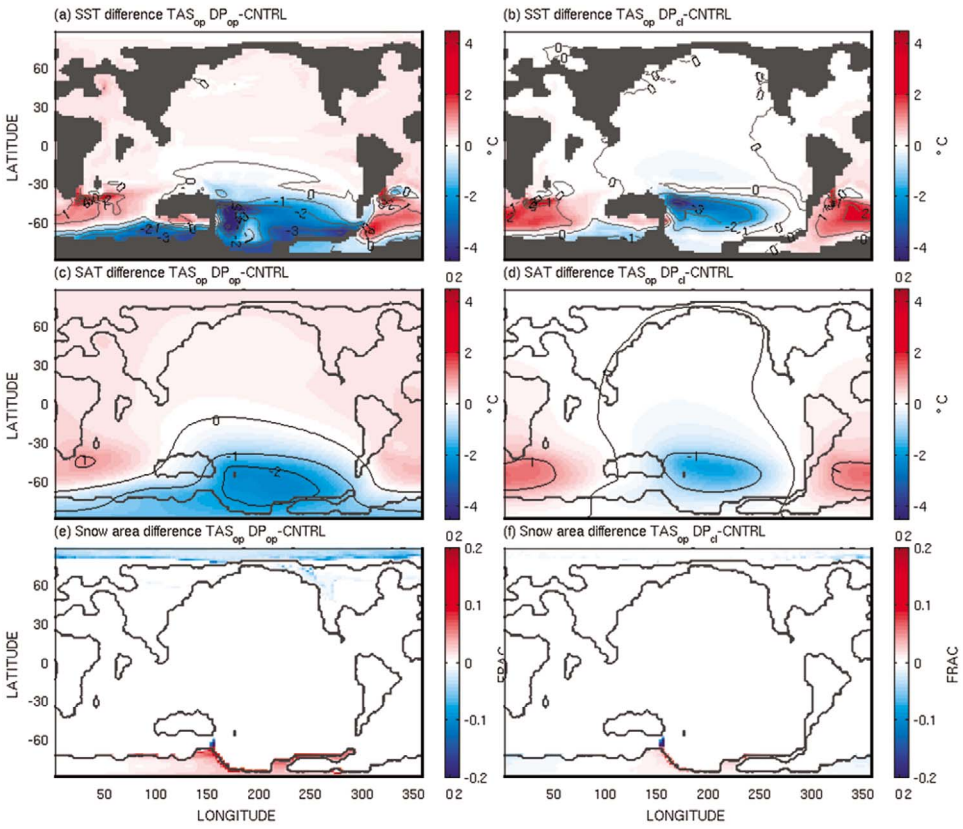

Figure 6. Annually averaged difference with CNTRL in sea surface temperature (Figures 6a and 6b, °C), surface air temperature (Figures 6c and 6d, °C) and snow area fraction (Figures 6e and 6f, fraction 0–1). Shown are TAS$_{op}$ DP$_{op}$ - CNTRL (left column) and TAS$_{op}$ DP$_{cl}$ - CNTRL (right column).

Australo-Antarctic Gulf. The large subtropical gyre between Australia and Drake Passage is reduced in strength from 50 Sv to 20 Sv.

[26] Figure 6 shows that deepening the Tasman Gateway in the Eocene simulation leads to significant circumpolar SST cooling of up to 3°C close to Antarctica in TAS$_{op}$ DP$_{op}$ (Figure 6a), while high latitude cooling is significantly less in TAS$_{op}$ DP$_{cl}$ (Figure 6b). This indicates that the high latitude cooling is associated with the establishment of the Antarctic Circumpolar Current (ACC) in the unobstructed case TAS$_{op}$ DP$_{op}$. Mid-latitude cooling occurs only between Australia and South America, while the mid southern latitudes warm elsewhere. There is a warming of up to 0.5°C throughout the world ocean in TAS$_{op}$ DP$_{op}$ and there is no northern hemisphere cooling. Clearly, the SST cooling pattern arising from the deepening of the Tasman Seaway in our model can not be associated with the global cooling pattern found in proxies [*Liu et al.*, 2009]. In particular, the slight northern hemisphere warming (Figure 6a), Arctic sea ice reduction (Figure 6e) and absence of winter-time cooling (figure not shown) is contrary to the marked sea-ice induced terrestrial winter cooling on Greenland found by *Eldrett et al.* [2009]. Furthermore, the 2.5°C tropical SST cooling inferred from Tanzanian Drilling Project sites 11, 12 and 17 across the Eocene/Oligocene transition found by *Lear et al.* [2008] is not reproduced by merely deepening the Tasman Seaway in our model. Finally, the 5°C cooling found at high latitude OPD sites in both hemispheres by *Liu et al.* [2009] (sites 336 and 511 in particular) is also not reproduced. The lack of low-latitude cooling in response to deepening the Tasman Seaway, along with a lack of bipolar response further indicates the need to invoke additional drivers (e.g. changes in atmospheric pCO_2) and feedbacks (e.g. clouds) to explain the global Cenozoic cooling, including the Eocene-Oligocene transition.

[27] Warming between Australia and South America in TAS$_{op}$ DP$_{op}$ occurs in conjunction with a cooling to the south at these longitudes. This increase in latitudinal temperature gradient is associated with the replacement of the large subpolar gyre there with a zonal current. The latitudinal heat transport associated with the gyre circulation reduces the latitudinal temperature gradient across the gyre, whereas the zonal circulation in TAS$_{op}$ DP$_{op}$ is associated with a stronger front across it. This argument can not be applied to the Ross Sea gyre. As in the case of the larger gyre, the Ross Sea gyre cools East Australia by advecting high latitude water northwards. This influence is replaced by water originating from somewhat lower latitudes in the Australo-Antarctic Gulf in TAS$_{op}$ DP$_{op}$ (Figure 5). As in the case of the other gyre, the lower latitude origin of the northward flowing water would suggest a warming east of Australia. However, this warming is strongly restricted to the south coast of Australia and the coastal region east of the land bridge, and cooling dominates further off shore. This is because the northward flow in the Ross Gyre in this area is weak, whereas the circumpolar flow through the Australo-

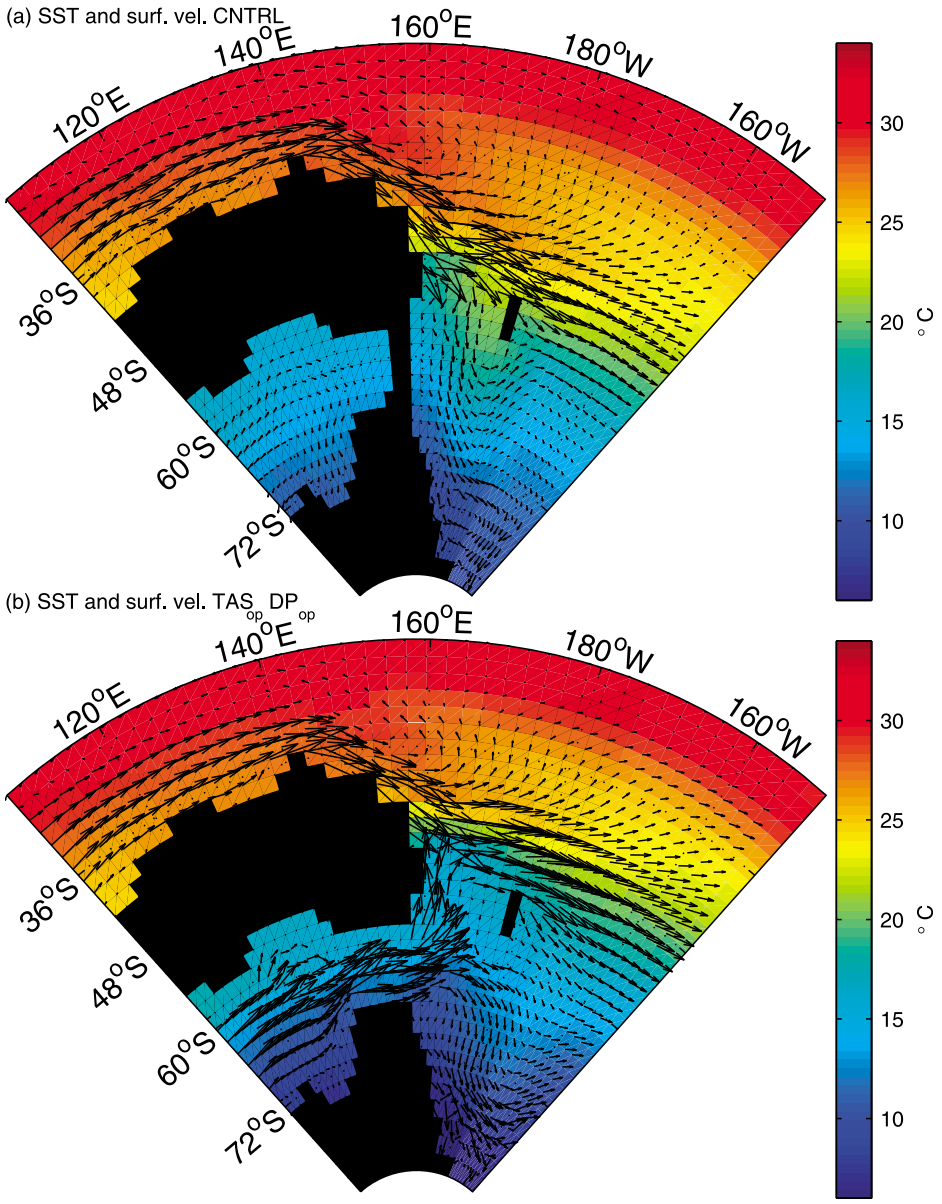

Figure 7. Sea surface temperature (SST) in the vicinity of Australia with surface velocity vectors overlaid for (a) CNTRL and (b) TAS_{op} DP_{op}.

Antarctic Gulf is strong (figure of velocities not shown). The higher rate of northward flow reduces the influence of the subtropical gyre to the north, cooling the region. We will see later that the thermocline flow is opposite to the barotropic flow in this region.

[28] The warming south of Australia and east of the land bridge includes OPD Site 1172 examined by *Stickley et al.* [2004], who find that the development of the Tasman Seaway during the earliest Oligocene leads to warming there, and attribute this to an increasing influence of a proto-Leeuwin current passing through the Australo-Antarctic Gulf. This is in good agreement with our model results. However, in contrast to the inferences for the wider effect of the inception of the ACC based on Site 1172 by *Stickley et al.* [2004], we find that cooling does occur further to the south and to the east of this site in our model. The SST cooling immediately off the Antarctic coast is modest and no greater than 3°C. The SST changes in response to deepening of the Tasman gateway in TAS_{op} DP_{op} leads to a very modest warming of up to only 0.4°C in the zonal mean over Antarctica. This shows that the climatic effect of the deepening of the Tasman gateway under realistic Eocene forcing is weak in the model (Figure 6c). As a result, there is only a very moderate Antarctic snow cover increase in TAS_{op} DP_{op} (Figures 6e and 6f), and a decrease in Arctic sea ice. Clearly, Antarctic glaciation could not be initiated by the deepening of the Tasman Seaway alone in this model at 1500 ppm pCO_2.

[29] Figures 7 and 8 show the SST and ocean velocities at the surface and 460 m depth around Australia. When the Tasman Gateway is closed, surface flow is southward along Australia's east coast and also the land bridge across the Tasman Seaway (Figure 7a), whilst northward flow associated with the Ross Sea gyre is restricted east of New

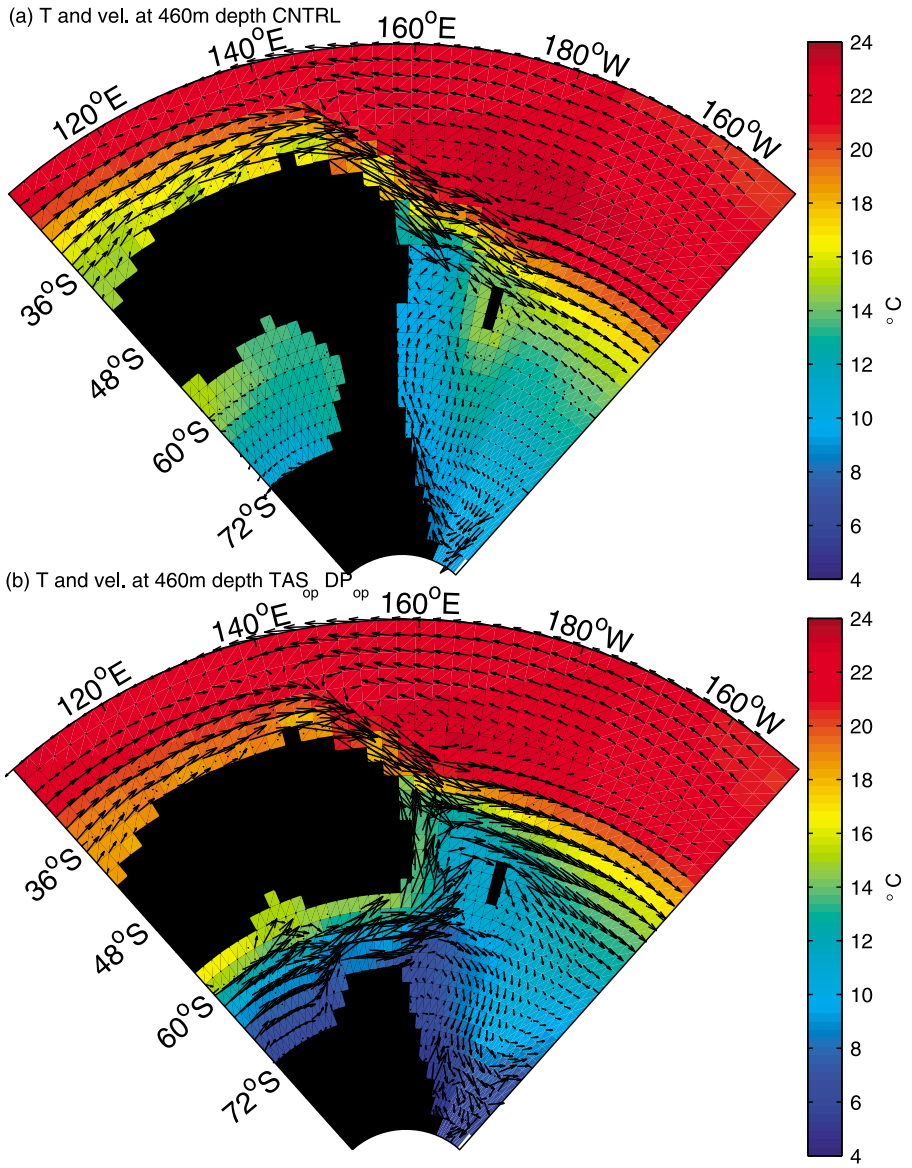

Figure 8. Sea temperature at 460 m in the vicinity of Australia with local velocity vectors overlaid depth for (a) CNTRL and (b) TAS_{op} DP_{op}.

Zealand. In contrast, the northward main flow direction east of Australia immediately below the surface is contrary to this shallow surface flow (see Figure 8a). Indeed, this northward flow is in agreement with the northward direction of the Ross Sea gyre seen in the bartropic stream function (see Figure 5).

[30] Deepening the Tasman gateway leads to the replacement of the warm southward surface flow by a much stronger northward flow originating from the Australo-Antarctic Gulf, leading to warming close to the Australian coast but significant cooling elsewhere in the Ross Sea gyre area. At depth (e.g. 460 m), a weak northward velocity associated with the Ross Sea gyre is replaced by a more vigorous northward flow associated with the ACC (Figure 8b). This leads to cooling there due to the difference in mass transport between the two currents, whereby the current originating from the Australo-Antarctic Gulf delivers cool high latitude water to more equatorward latitudes at a greater rate. Therefore, the east Australian warming suggested by *Huber et al.* [2004] to result from the deepening of the Tasman Seaway is limited to close to the Australian coast, and cooling prevails further off shore. Finally, the emergence of the ACC is associated with a doubling of the SST gradient across the Australo-Antarctic Gulf, from 4°C to 8°C, leading to less uniform temperature conditions in this sea.

[31] The surface flow east of Australia is contrary to the simulations of *Huber et al.* [2004], who diagnosed a northward flow throughout the water column up to and including the surface in a coupled simulation with Eocene geometry. However, our flow agrees with that of *Huber et al.* [2004] immediately below the surface (460 m, see Figure 8) and the barotropic stream function (Figure 5) also agrees with their study. The difference in surface flow between the two models may arise from the difference in polarity of deep sinking between our simulations and those of *Huber et al.* [2004], as deep sinking in the Ross Sea has a

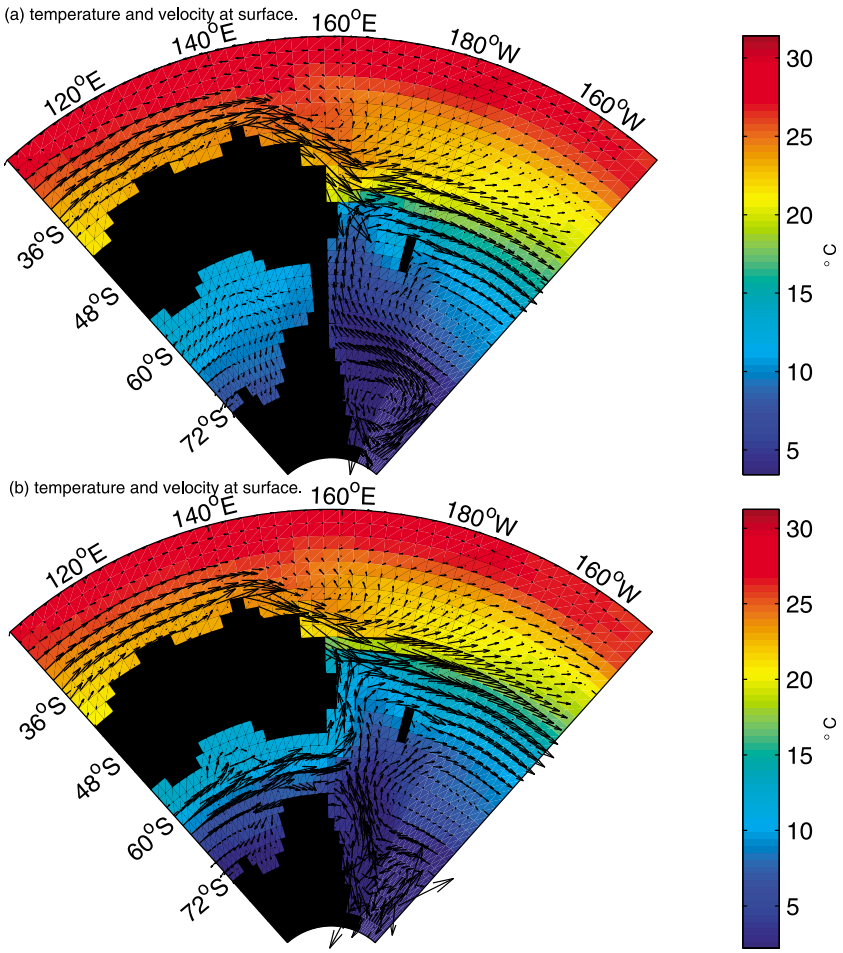

Figure 9. Sea surface temperature in experiments with suppressed Ross Sea sinking for (a) CNTRL and (b) TAS_{op} DP_{op} in the vicinity of Australia with surface velocity vectors overlaid.

potential to influence the local horizontal flow structure. Differences in gyre circulation with *Huber et al.* [2004] are likely to arise from differences in deep sinking, as our ocean wind stress is identical to theirs. To examine the reasons for the vertical change in flow direction in CNTRL, we have conducted additional simulations of CNTRL and TAS_{op} DP_{op} where additional fresh water is added to the Ross Sea in order to suppress deep sinking there. In response, there is now 32 Sv of northern sinking in CNTRL. The suppression of Ross Sea sinking leads to a strong northward western boundary current along the land bridge between Australia and Antarctica in CNTRL (Figure 9a). This surface circulation is now in agreement with *Huber et al.* [2004] and is similar to the vertically averaged flow. This result demonstrates that deep Ross Sea sinking in the standard CNTRL simulation exerts an influence on the surface circulation there via the local density gradients. This causes a baroclinic velocity component with sufficient vertical shear to neutralize the mean flow at the surface. Closer examination of temperature and density in this region show that a significant zonal temperature and density gradient exists east of the Tasman land bridge in the standard CNTRL simulation around 460 m depth, but is absent from the modified CNTRL simulation where deep Ross Sea sinking is suppressed (figure not shown). Denser water is found closer to the land bridge in the standard CNTRL simulation, while density decreases further off shore. The associated surface steric height gradient gives results in a meridional velocity field that increases in the southward directionas the surface is approached from below, due to the thermal wind relationship. This shows that the local density distribution around Antarctica may influence surface currents there, accounting for localized flow differences between our study and that of *Huber et al.* [2004].

[32] Antarctic cooling as a result of the deepening of the Tasman Seaway is largely independent of the detailed Ross Sea circulation, as shown in Figure 10 where the sea surface temperature difference between TAS_{op} DP_{op} and the modified CNTRL experiment is shown. With deep sinking in the Ross Sea suppressed, there is now significant local warming east of Australia instead of cooling. Deep cooling remains similar (around 3°C), however, regardless of the suppression of Ross Sea sinking (figure not shown). In this modified CNTRL experiment, deep ventilation occurs elsewhere around Antarctica (18 Sv), allowing Antarctic cooling to be reflected in deep ocean temperature changes, regardless of the local circulation in the Ross Sea.

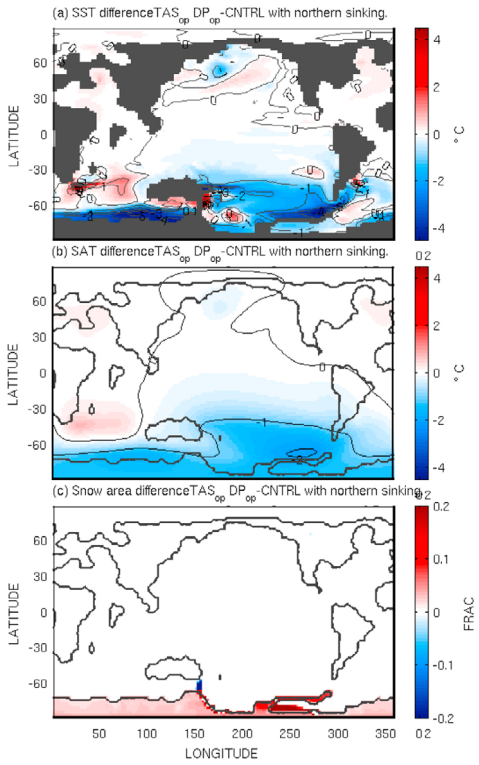

Figure 10. Annually averaged difference between the modified TAS$_{op}$ DP$_{op}$ and CNTRL experiment in (a) sea surface temperature, (b) surface air temperature and (c) snow area. An extra FW flux has been added to stimulate northern sinking in both simulations.

3.3. Changes in Vertical Ocean Structure

[33] The Eocene global volume averaged sea temperature in CNTRL is 10.7°C, a 7.0°C increase above PD. The Eocene deep ocean temperature below 3000 m depth is at an average of 9.2°C, a 7.3°C increase above the PD value of 1.9°C. This value lies within the Eocene deep ocean temperature range of 12°C during the Early Eocene Climatic Optimum and 6° at the late Eocene found by *Zachos et al.* [2001]. *Huber et al.* [2003] found a 7°C warmer deep ocean in their 560 ppm Eocene run, indicating that deep ocean warming can be achieved even with modest atmospheric CO_2. Their overturning circulation is different from ours, with more water sinking in the Northern Hemisphere and fresher conditions in the Southern Ocean, and so changes in deep ocean temperatures may not be readily compared. Figure 11 shows the zonal mean potential temperature for CNTRL and TAS$_{op}$ DP$_{op}$ and Figure 13 shows the vertical profile of globally averaged ocean potential temperature. In agreement with previous studies where an ACC is absent [e.g., *Sijp and England*, 2004], the warm deep ocean conditions between 9.5–10°C in CNTRL (Figures 11a and 13a) are vertically rather homogeneous, and the thermocline is shallow. Deep ocean temperature below 3000 m depth is 9.1°C in the Eocene CNTRL run, and cools by about 3°C (Table 2 and Figures 11c and 13b) to reach 6.3°C upon the deepening of the Tasman gateway in TAS$_{op}$ DP$_{op}$. Of note, the Drake Passage needs to be open already to achieve deep ocean cooling, as we find a much more modest deep ocean cooling of only 0.9°C when Drake Passage remains closed during the deepening of the Tasman Seaway (Figure 12a) in TAS$_{op}$ DP$_{op}$. In this case MOC changes remain minor (figure not shown), indicating that changes in source region properties are a main driver of deep ocean temperature changes. In the standard experiment TAS$_{op}$ DP$_{op}$ the MOC is reduced, but changes in source region temperatures dominate the effect on the deep ocean. In this case a reduction in deep sinking in the absence of other changes would more likely warm the deep ocean than cool it, although a deeper discussion of this topic is beyond the scope of this paper.

[34] As in the experiments of *Toggweiler and Bjornsson* [2000] and *Sijp and England* [2004], the establishment of the ACC leads to a deepening of the isotherms north of the current due to thermal wind balance. Therefore, the modest warming of the world ocean north of the ACC (Figure 6) and the thermocline warming up to 1°C (Figure 11c) is associated with the establishment of the ACC. Despite the deepening of the thermocline, the deepening of the Tasman Seaway leads to a globally volume-averaged temperature cooling of 2.1°C from 10.7°C to 8.6°C (Table 2). The appearance of an ACC (albeit modest) in TAS$_{op}$ DP$_{op}$ leads to the establishment of a weak deep vertical ocean temperature gradient (Figure 13b). This gradient is a well-established feature for the present day ocean and also a feature of the PD experiments.

[35] The use of a simple atmospheric energy balance model and a non-interactive wind field in our experiments precludes an interactive wind response. The Eocene winds used here are characterized by weaker SH westerlies than present-day condition. To examine the effect of a possible strengthening of the SH westerlies on the inception of the ACC, we have also run an extra simulation TAS$_{op}$ DP$_{op}$ WINDS, where present-day winds replace the Eocene winds in the TAS$_{op}$ DP$_{op}$ case, representing the effect of strengthened westerlies in response to an enhanced temperature gradient and terrestrial ice-growth associated with the gateway deepening (Figure 11b). Present-day winds are in known equilibrium with cooler conditions and Antarctic land ice. This approach allows us to make use of the simplicity of our atmospheric model to capture a range of possible climate responses. As seen in Figure 12b, our results are somewhat more pronounced when strengthened westerly winds are included. Deep ocean cooling remains between 3–4°C, but the enhanced ACC leads to a further deepening of the thermocline to the north, now reaching maxima of 2°C warming. The total oceanic response to the deepening of the Tasman Seaway likely involved a significant deepening of the thermocline to the north, regardless of a possible onset of significant NH sinking, a feature absent in our TAS$_{op}$ DP$_{op}$ simulations.

[36] The deepening of the Tasman Seaway to 1300 m depth in our Eocene model leads to a 3°C cooling of the deep ocean below 3000 m depth and the establishment of a 66 Sv ACC. No initiation of Northern Component Water is found, indicating that an overturning polarity change may require further bathymetric changes allowing a more mature ACC to develop. Additionally, a deepening of North Atlantic sills may also facilitate the onset of North Atlantic sinking. Our 1500 ppm Eocene CNTRL simulation yields a

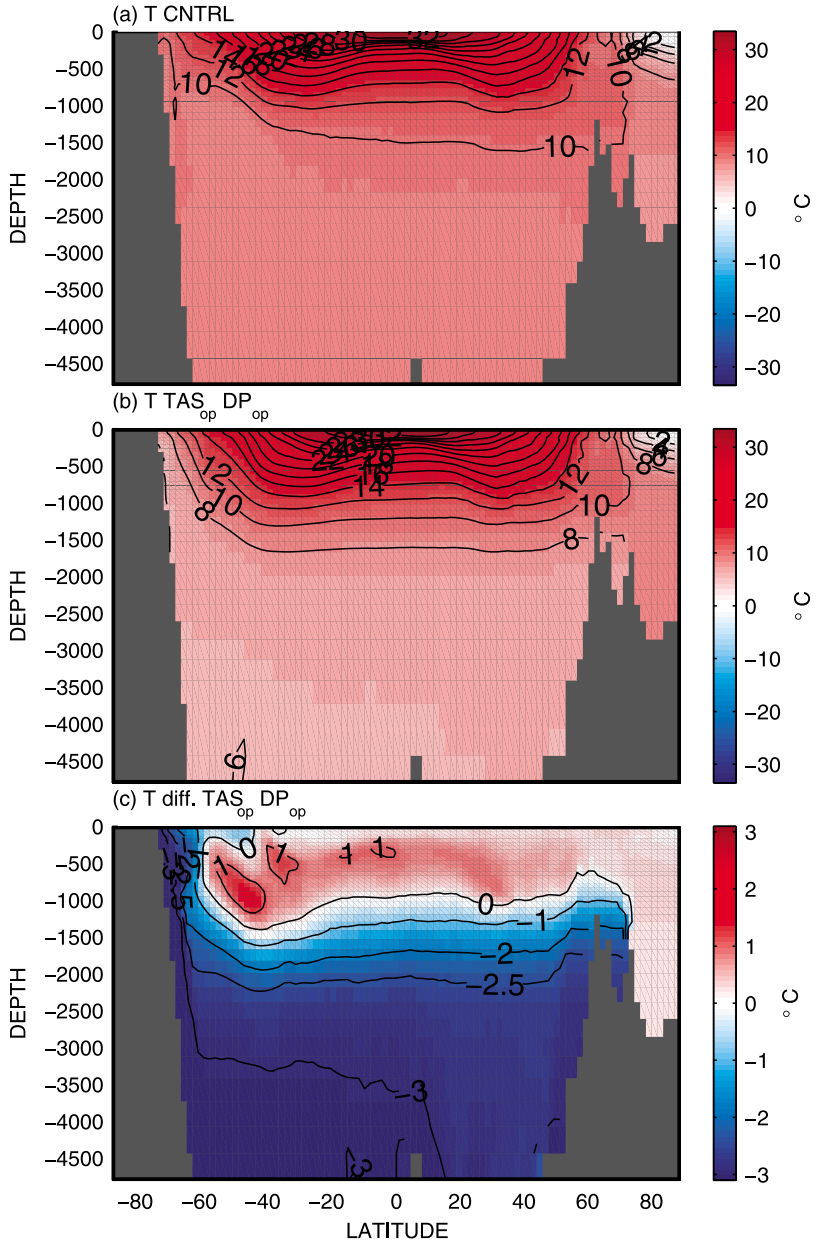

Figure 11. Zonally averaged ocean temperature (°C) for (a) CNTRL, (b) TAS$_{op}$ DP$_{op}$ and (c) difference TAS$_{op}$ DP$_{op}$ - CNTRL.

warm and ice-free climate. Average SST is 25.8°C in our CNTRL Eocene run, a 8.3°C increase over PD. The deepening of the Tasman Seaway has no global climatic effect, but localized cooling does arise around Antarctica due to the thermal isolation by a proto ACC if Drake Passage is also open. A deep and relatively wide Drake Passage as we have used here is of debatable accuracy for the Eocene-Oligocene transition. Since the deep ocean is ventilated only from high latitudes this localized surface cooling leads to significant global deep ocean cooling. This shows that deep ocean temperature changes arising from tectonic events need not reflect widespread (global) climatic change at the surface, nor a polarity shift in deep sinking. It also suggests that benthic temperature records are a poor guide to global mean surface temperatures. The gateway-related benthic cooling of 3°C in our model is comparable in magnitude to the 4°C deep ocean cooling simulated by *Liu et al.* [2009] as a result of a drop in pCO_2 at the end of the Eocene. Consequently, while gateway changes may play only a minor role in explaining Antarctic temperature changes they potentially play as large a role as greenhouse gas changes in explaining benthic temperature trends.

4. Summary and Conclusions

[37] We have found that the deepening of the Tasman Seaway in the presence of an open Drake Passage and the associated establishment of the Antarctic Circumpolar Current (ACC) have a moderate climatic impact on Antarctica. Despite 1–2°C continental cooling, no glaciation

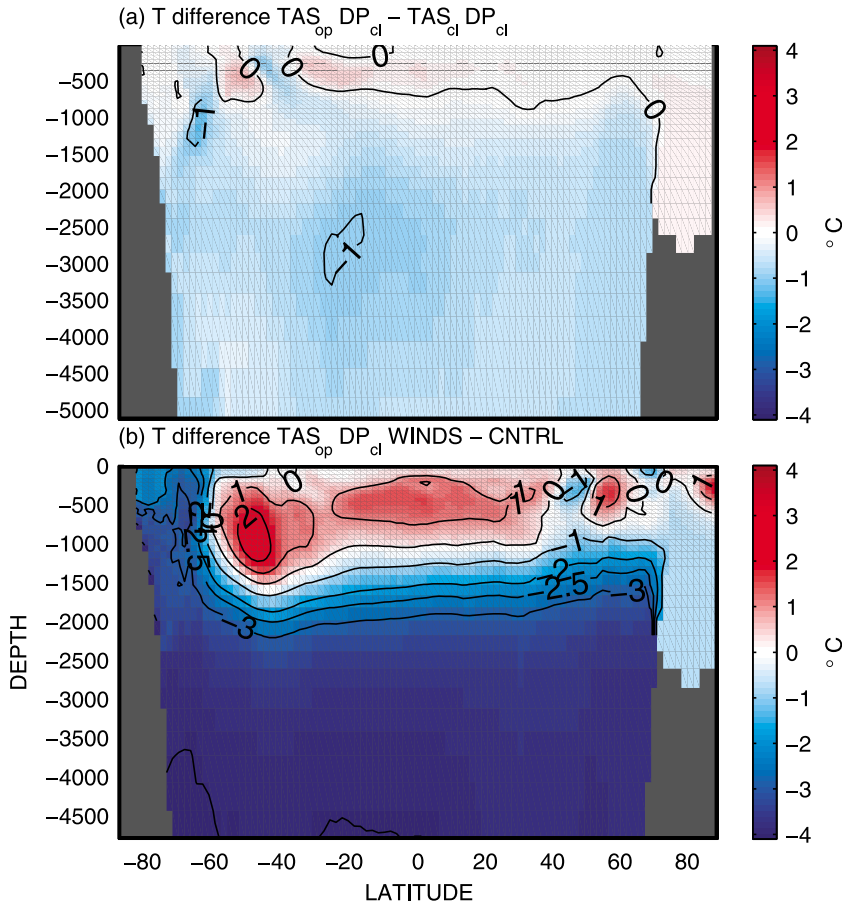

Figure 12. Zonally averaged sea temperature (°C) difference (a) TAS$_{op}$ DP$_{cl}$ - TAS$_{cl}$ DP$_{cl}$ and (b) TAS$_{op}$ DP$_{op}$ WINDS - CNTRL. In the TAS$_{op}$ DP$_{op}$ WINDS experiments Eocene winds are replaced by present-day winds, while CNTRL remains unaltered.

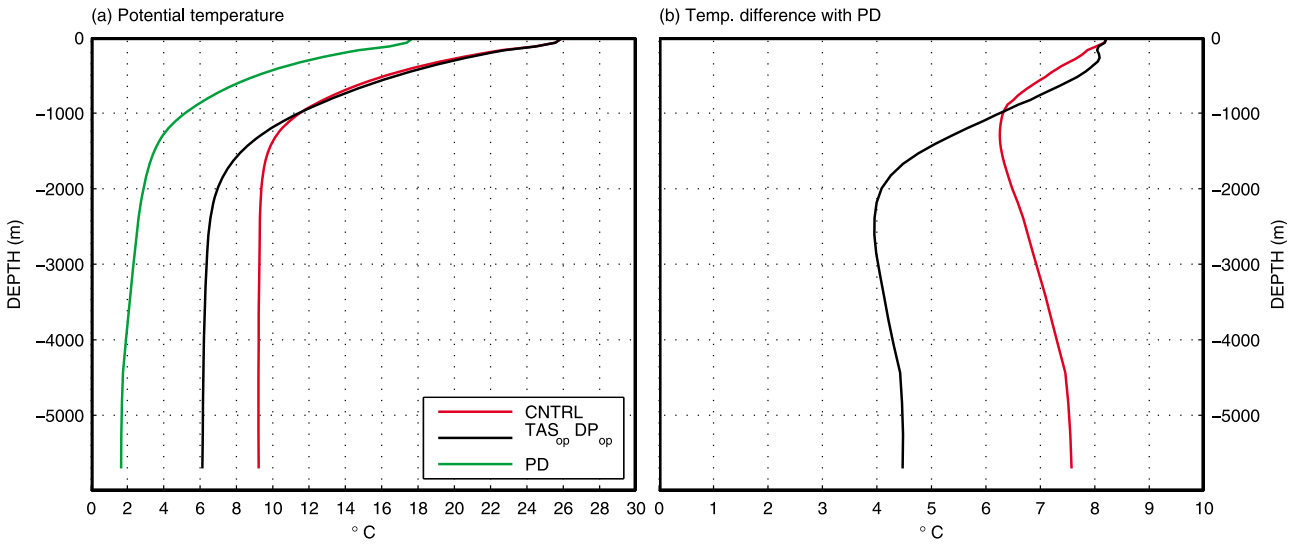

Figure 13. Vertical profile of global average (a) ocean potential temperature and (b) potential temperature difference (relative to PD) for CNTRL (red) and TAS$_{op}$ DP$_{op}$ (black). Included in Figure 13a are the present day values (PD, green).

occurs in response to opening the Tasman Seaway to deep geostrophic flow. Nonetheless, locally, the Antarctic deep sinking regions cool sufficiently to lead to a global deep ocean cooling of 3°C. The lack of Antarctic glaciation lends further support to the idea that atmospheric pCO_2 Changes rather than gateway changes preconditioned the climate for Antarctic glaciation and global cooling across the Eocene/Oligocene transition [e.g., *DeConto and Pollard*, 2003; *Huber et al.*, 2004; *Liu et al.*, 2009]. No initiation of Northern Component Water is found, indicating that this may require the development of a more mature ACC.

[38] For reference, our findings can be summarized by the following main points:

[39] 1. The deep ocean undergoes a significant cooling.

[40] 2. Such deep ocean changes can occur without a transition in the global surface climate.

[41] 3. Surface ocean temperatures around Antarctica cool. Benthic cooling reflects this localized Antarctic SST response arising from the oceanic thermal isolation of Antarctic waters south of an emerging proto-ACC.

[42] 4. The thermocline deepens north of the ACC.

[43] 5. Unlike the modern-day geometry DP experiments [see *Sijp and England*, 2009], no transition to a NH overturning state is required to obtain this benthic cooling and a thermal isolation of Antarctica. This is an overlooked but important conclusion, as some studies invoke the onset of Northern Component Water as a critical factor in cooling Antarctica.

[44] 6. The replacement of the Ross Sea gyre by a proto-ACC does not warm the entire region east of Australia (with the exception of a small coastal margin) in our standard CNTRL experiment. In contrast, when we suppress deep Ross Sea sinking we find significant warming instead of cooling east of Australia.

[45] 7. We find a much more modest deep ocean warming of only 0.9°C when Drake Passage is closed during the deepening of the Tasman Seaway.

[46] Compared to the effect of deepening the Tasman Seaway in this study, *Sijp et al.* [2009] find a stronger and more uniform Antarctic SST cooling (around 4–5°C on average for 1500 ppm pCO_2) when they open Drake Passage under a present-day bathymetry. The much greater spatial extent of their SST cooling leads to an Antarctic SAT cooling of 7°C on average, much greater than the 1°C SAT cooling found here. The greater temperature response found by *Sijp et al.* [2009] arises from a stronger reduction in Antarctic sinking, combined with the onset of northern hemisphere sinking when Drake Passage is opened.

[47] The Antarctic SST cooling in response to the inception of a proto-ACC also occurs in our altered experiments where deep Ross Sea sinking is suppressed and the southeastern part of Australia is under the influence of a clockwise proto-Ross Sea gyre, as described by *Huber et al.* [2004]. This shows that the East Australia Current and its subsequent deflection by the inception of the ACC are not required to explain the thermal isolation of Antarctica in response to the deepening of the Tasman Seaway. Instead, the emergence of an ACC leads to Antarctic SST cooling regardless of whether before the deepening the East Australia Current reached close to the Antarctic continent.

[48] The development of the ACC requires the deepening of Drake Passage and the Tasman Seaway, and is likely to have taken place over a prolonged period of time [see, e.g., *Livermore et al.*, 2004; *Stickley et al.*, 2004; *Livermore et al.*, 2005; *Lagabrielle et al.*, 2009], whereas the Eocene/Oligocene transition constitutes a rather narrow time interval. We do not interpret our deep ocean cooling result as a sudden event. Furthermore, the total deep sea cooling from the middle Eocene to present is estimated to be approximately 12°C [*Lear et al.*, 2000; *Miller et al.*, 2009], significantly exceeding the cooling found here (3°C). Our results do nonetheless suggest that the development of an ACC occurred somewhere within this interval (closer to the E-O boundary than to the present-day) and that this favored cooler benthic temperatures. Furthermore, a deepening of the thermocline also occurred during this period. These changes could possibly entail significant changes on ocean biochemistry and carbon uptake.

[49] The deepening of the thermocline north of the circumpolar ocean and the modest increase in vertical abyssal temperature gradient in response to opening the Tasman Seaway suggests an increased partitioning of the ocean structure into a surface layer, an intermediate layer and a deep/bottom layer. This is reminiscent of findings by *Katz et al.* [2011], who describe the development of the modern 4-layer ocean structure during the early Oligocene under the gradual development of the ACC. However, the deep layer in that study is thought tobe ventilated from the north, whereas we find mostly southern ventilation. *Scher and Martin* [2008] infer an increase in ACC throughflow at the early/late Oligocene boundary. They link an increasing ACC with increasing Northern Component Water (NCW), and conclude that export of NCW to the Southern Ocean increased in the late Oligocene with the development of a mature ACC. Our findings suggest that, in addition to the opening of the Tasman Seaway, further factors such as North Atlantic bathymetric changes are needed to explain the trend of increasing NCW outflow during the Oligocene and Miocene. As a result, our TAS_{op} DP_{op} experiments may be more relevant to the very early (rather than later) Oligocene. Nonetheless, we show that even in the absence of strong NCW outflow, significant deep ocean cooling could occur merely in response to the development of a proto-ACC. Also, further deepening and widening than shown here may be needed to obtain an ACC that is more conducive of NCW outflow. Note that our alternative experiments where the Tasman Seaway is opened in the presence of northern sinking (Ross Sea sinking suppressed) exhibit a significant increase in northern sinking (figure not shown), and indicate that the presence of an ACC stimulates northern sinking when possible.

[50] *Tigchelaar et al.* [2010] invoke a shift from southern sinking to bipolar sinking to explain the first cooling step at the E-O transition and outline possible causes for this shift, for instance changes in the Greenland-Scotland Ridge and decreasing pCO_2. Such changes do occur, but these same fluctuations could also easily return the system to its original state. Our results show that an inception of northern sinking may not be needed to explain deep ocean cooling during the E/O transition. Instead, the deepening of southern gateways alone may lead to deep ocean cooling. Another possibility more in line with *Tigchelaar et al.* [2010] is that the deepening of the thermocline north of the young ACC, associated with the deepening of SO gateways preconditioned the

world ocean for a transition to deep sinking in both hemispheres. The hydrological cycle in our model precludes this transition in the experiments shown here, but alternative versions of our experiments where the hydrological cycle is slightly altered demonstrate the plausibility of this scenario (figure not shown).

[51] The weak global climatic response to the deepening of the Tasman Seaway in our model is in overall agreement with the contention of *DeConto and Pollard* [2003] and *Huber et al.* [2004] that global warmth associated with high atmospheric greenhouse gas concentrations was the main cause of the mild and ice-free Antarctic conditions during hot house climates such as the Eocene. Nonetheless, the deepening of the Tasman Seaway leads to significant local and global benthic cooling. The strongest cooling occurs around New Zealand, where sea surface temperature drops by approximately 4°C in response to a deepening of the Tasman Gateway. Therefore, interpretations of deep ocean temperature changes across the Eocene/Oligocene boundary need to take the direct effect of the deepening of the Tasman Seaway into consideration.

[52] **Acknowledgments.** We thank the University of Victoria staff for support in usage of the their coupled climate model. This research was supported by the Australian Research Council and the Australian Antarctic Science Program. Matthew Huber is supported by U.S. National Science Foundation (NSF) grant 0927946-ATM. This is Purdue Climate Change Research Center Publication 1111. We thank Andreas Oschlies for hosting a visit to IFM-GEOMAR and supplying code and advice to allow W. P. Sijp to implement the turbulent kinetic energy scheme of *Blanke and Delecluse* [1993] based on *Gaspar et al.* [1990] into the model. We thank Sascha Flögel for stimulating discussions and detailed comments on this manuscript.

References

Abbot, D., M. Huber, G. Bousquet, and C. C. Walker (2009), High-CO_2 cloud radiative forcing feedback over both land and ocean in a global climate model, *Geophys. Res. Lett.*, *36*, L05702, doi:10.1029/2008GL036703.

Ali, J. R., and M. Huber (2010), Mammalian biodiversity on Madagascar controlled by ocean currents, *Nature*, *463*, 653–656.

Barker, P. F., and J. Burrell (1977), The opening of Drake Passage, *Mar. Geol.*, *25*, 15–34.

Berggren, W. A., and C. D. Hollister (1977), Plate tectonics and paleocirculation–Commotion in the ocean, *Tectonophysics*, *38*, 11–48.

Bijl, P. K., S. S. Schouten, and A. Sluijs (2009), Early palaeogene temperature evolution of the southwest Pacific Ocean, *Nature*, *461*, 776–779.

Blanke, B., and P. Delecluse (1993), Variability of the tropical Atlantic Ocean simulated by a general circulation model with two different mixed-layer physics, *J. Phys. Oceanogr.*, *23*, 1363–1388.

Corfield, R. M., and R. D. Norris (1996), Deep water circulation in the Paleocene Ocean, *Geol. Soc. Spec. Publ.*, *101*, 443–456.

Coxall, H. K., and P. N. Pearson (2007), The Eocene-Oligocene transition, in *Deep Time Perspectives on Climate Change: Marrying the Signal From Computer Models and Biological Proxies*, edited by M. Williams et al., pp. 351–387, Geol. Soc. of London, Bath, London.

Coxall, H. K., et al. (2005) Rapid stepwise onset of Antarctic glaciation and deeper calcite compensation in the Pacific Ocean, *Nature*, *433*, 53–57.

Cramer, B. S., J. R. Toggweiler, J. D. Wright, M. E. Katz, and K. G. Miller (2009), Ocean overturning since the Late Cretaceous: Inferences from a new benthic foraminiferal isotope compilation, *Paleoceanography*, *24*, PA4216, doi:10.1029/2008PA001683.

DeConto, R. M., and D. Pollard (2003) Rapid Cenozoic glaciation of Antarctica induced by declining atmospheric CO_2, *Nature*, *421*, 245–248.

DeConto, R. M., et al. (2008), Thresholds for Cenozoic bipolar glaciation, *Nature*, *455*, 652–656.

Eldrett, J. S., D. R. Greenwood, I. C. Harding, and M. Huber (2009), Increased seasonality through the eocene to oligocene transition in northern high latitudes, *Nature*, *459*, 969–974.

Gaspar, P., Y. Gregoris, and J. M. Lefevre (1990), A simple eddy kinetic energy model for simulations of the oceanic vertical mixing: Tests at station papa and long-term upper ocean study site, *J. Geophys. Res.*, *95*, 16,179–16,193.

Gent, P. R., and J. C. McWilliams (1990), Isopycnal mixing in ocean general circulation models, *J. Phys. Oceanogr.*, *20*, 150–155.

Gleason, J. D., D. J. Thomas, T. C. Moore, J. D. Blum, R. M. Owen, and B. A. Haley (2009), Early to middle Eocene history of the Arctic Ocean from Nd-Sr isotopes in fossil fish debris, Lomonosov Ridge, *Paleoceanography*, *24*, PA2215, doi:10.1029/2008PA001685.

Huber, M., and D. Nof (2006), The ocean circulation in the southern hemisphere and its climatic impacts in the Eocene, *Palaeogeogr. Palaeoclimatol. Palaeoecol.*, *231*, 9–28.

Huber, M., and L. C. Sloan (2001), Heat transport, deep waters and thermal gradients: Coupled simulation of an Eocene "greenhouse" climate, *Geophys. Res. Lett.*, *28*, 3481–3484.

Huber, M., L. C. Sloan, and C. Shellito (2003), Early Paleogene oceans and climate: A fully coupled modeling approach using the NCAR CCSM, in *Causes and Consequences of Globally Warm Climates in the Early Paleogene*, edited by S. L. Wing et al., *Geol. Soc. Spec. Publ.*, *369*, 25–47.

Huber, M., H. Brinkhuis, C. E. Stickley, K. Doos, A. Sluijs, J. Warnaar, S. A. Schellenberg, and G. L. Williams (2004), Eocene circulation of the Southern Ocean: Was Antarctica kept warm by subtropical waters?, *Paleoceanography*, *19*, PA4026, doi:10.1029/2004PA001014.

Katz, M. E., K. G. Miller, J. D. Wright, B. S. Wade, J. V. Browning, B. S. Cramer, and Y. Rosenthal (2008), Stepwise transition from the Eocene greenhouse to the Oligocene icehouse, *Nature*, *1*, 329–334.

Katz, M. E., et al. (2011), Impact of Antarctic Circumpolar Current development on late Paleogene ocean structure, *Science*, *332*, 1076–1079.

Kennett, J. P. (1977), Cenozoic evolution of Antarctic glaciation, the Circum Antarctic Ocean, and their impact on global paleoceanography, *J. Geophys. Res.*, *82*, 3843–3860.

Lagabrielle, Y., et al. (2009), The tectonic history of drake passage and its possible impacts on global climate, *Earth Planet. Sci. Lett.*, *279*, 197–211.

Lawver, L. A., and L. M. Gahagan (1998), *Opening of Drake Passage and its Impact on Cenozoic Ocean Circulation*, pp. 212–226, Oxford Univ. Press, New York.

Lear, C. H., H. Elderfield, and P. A. Wilson (2000), Cenozoic deep-sea temperatures and global ice volumes from Mg/Ca in benthic foraminiferal calcite, *Science*, *287*, 269–272.

Lear, C. H., T. R. Bailey, P. N. Pearson, H. K. Coxall, and Y. Rosenthal (2008), Cooling and ice growth across the Eocene-Oligocene transition, *Geology*, *36*, 251–254.

Liu, Z., et al. (2009), Global cooling during the Eocene-Oligocene climate transition, *Science*, *323*, 1187–1190.

Livermore, R., R. Eagles, G. Morris, and P. A. Maldonado (2004), Shackleton fracture zone: No barrier to early circumpolar circulation, *Geology*, *32*, 797–800.

Livermore, R., A. Nankivell, G. Eagles, and P. Morris (2005), Paleogene opening of Drake Passage, *Earth Planet. Sci. Lett.*, *236*, 459–470.

Mikolajewicz, U., E. Maier-Reimer, T. J. Crowley, and K. Y. Kim (1993), Effect of Drake Passage and Panamanian gateways on the circulation of an ocean model, *Paleoceanography*, *8*, 409–426.

Miller, K. G., R. G. Fairbanks, and G. S. Mountain (1987), Tertiary oxygen isotope synthesis, sea level history, and continental margin erosion, paleoceanography, *Paleoceanography*, *2*, 1–19, doi:10.1029/PA002i001p00001.

Miller, K. G., J. D. Wright, and R. G. Fairbanks (1991), Unlocking the ice house: Oligocene-Miocene oxygen isotopes, eustasy, and margin erosion, *J. Geophys. Res.*, *96*, 6829–6848, doi:10.1029/90JB02015.

Miller, K. G., J. D. Wright, M. E. Katz, B. S. Wade, J. V. Browning, B. S. Cramer, and Y. Rosenthal (2009), Climate threshold at the Eocene-Oligocene transition: Antarctic ice sheet influence on ocean circulation, *Geol. Soc. Spec. Publ.*, *452*, 169–178.

Najjar, R. G., G. T. Nong, D. Seidov, and W. H. Peterson (2002), Modeling geographic impacts on early Eocene ocean temperature, *Geophys. Res. Lett.*, *29*(15), 1750, doi:10.1029/2001GL014438.

Nong, G. T., R. G. Najjar, D. Seidov, and W. H. Peterson (2000), Simulation of ocean temperature change due to the opening of Drake Passage, *Geophys. Res. Lett.*, *27*, 2689–2692.

Pacanowski, R. (1995), *MOM 2 Documentation User's Guide and Reference Manual*, *GFDL Ocean Tech. Rep. 3.2*, 232 pp., NOAA, Princeton, N. J.

Pagani, M., J. C. Zachos, K. H. Freeman, B. Tripple, and S. Bohaty (2005), Marked decline in atmospheric carbon dioxide concentrations during the Paleogene, *Science*, *309*, 600–603.

Pearson, P. N., G. L. Foster, and B. S. Wade (2009), Atmospheric carbon dioxide through the Eocene-Oligocene climate transition, *Nature*, *461*, 1110–1113.

Scher, H. D., and E. E. Martin (2006), Timing and climatic consequences of the opening of Drake Passage, *Science*, *312*, 428–430.

Scher, H. D., and E. E. Martin (2008), Oligocene deep water export from the North Atlantic and the development of the Antarctic Circumpolar Current examined with neodymium isotopes, *Paleoceanography*, *23*, PA1205, doi:10.1029/2006PA001400.

Shackleton, N. J., et al. (1984), Oxygen isotope calibration of the onset of ice-rafting and history of glaciation in the North Atlantic region, *Nature*, *307*, 620–623.

Sijp, W. P., and M. H. England (2004), Effect of the Drake Passage throughflow on global climate, *J. Phys. Oceanogr.*, *34*, 1254–1266.

Sijp, W. P., and M. H. England (2005), On the role of the Drake Passage in controlling the stability of the ocean's thermohaline circulation, *J. Clim.*, *18*, 1957–1966.

Sijp, W. P., and M. H. England (2009), Atmospheric moisture transport moderates climatic response to the opening of Drake Passage, *J. Clim.*, *22*, 2483–2493.

Sijp, W. P., M. Bates, and M. H. England (2006), Can isopycnal mixing control the stability of the thermohaline circulation in ocean climate models?, *J. Clim.*, *19*, 5637–5651.

Sijp, W. P., M. H. England, and J. R. Toggweiler (2009), Effect of ocean gateway changes under greenhouse warmth. *J. Clim.*, *22*, 6639–6652.

Steph, S., R. Tiedemann, M. Prange, J. Groeneveld, D. Nürnberg, L. Reuning, M. Schulz, and G. H. Haug (2006), Changes in Caribbean surface hydrography during the Pliocene shoaling of the Central American Seaway, *Paleoceanography*, *21*, PA4221, doi:10.1029/2004PA001092.

Stickley, C. E., H. Brinkhuis, S. A. Schellenberg, A. Sluijs, U. Röhl, M. Fuller, M. Grauert, M. Huber, J. Warnaar, and G. L. Williams (2004), Timing and nature of the deepening of the tasmanian gateway, *Paleoceanography*, *19*, PA4027, doi:10.1029/2004PA001022.

Stickley, C. E., et al. (2009), Evidence for middle Eocene Arctic sea ice from diatoms and ice-rafted debris, *Nature*, *460*, 376–380.

Thomas, D. (2004), Evidence for deep-water production in the North Pacific Ocean during the early Cenozoic warm interval, *Nature*, *430*, 65–68.

Thomas, D., T. J. Bralower, and C. E. Jones (2003), Neodymium isotopic reconstruction of the late Paleocene-early Eocene thermohaline circulation, *Earth Planet. Sci. Lett.*, *209*, 309–322.

Tigchelaar, M., A. S. von der Heydt, and H. A. Dijkstra (2010), A new interpretation of the two-step $\delta^{18}O$ signal at the Eocene-Oligocene boundary, *Clim. Past Discuss.*, *6*, 1391–1419.

Toggweiler, J. R., and H. Bjornsson (2000), Drake Passage and paleoclimate, *J. Quaternian Sci.*, *15*, 319–328.

Via, R., and D. Thomas (2006), Evolution of Atlantic thermohaline: Early Oligocene circulation onset of deep-water production in the North Atlantic, *Geology*, *34*, 441–444.

von der Heydt, A., and H. A. Dijkstra (2006), Effect of ocean gateways on the global ocean circulation in the late Oligocene and early Miocene, *Paleoceanography*, *21*, PA1011, doi:10.1029/2005PA001149.

von der Heydt, A., and H. A. Dijkstra (2008), The effect of gateways on ocean circulation patterns in the Cenozoic, *Global Planet. Change*, *62*, 132–146.

Waddell, L. M., and T. C. Moore (2008), Salinity of the eocene arctic ocean from oxygen isotope analysis of fish bone carbonate, *Paleoceanography*, *23*, PA1S12, doi:10.1029/2007PA001451.

Weaver, A. J., et al. (2001), The UVic Earth System Climate Model: Model description, climatology, and applications to past, present and future climates, *Atmos. Ocean*, *39*, 1067–1109.

Zachos, J., and L. R. Kump (2005), Carbon cycle feedbacks and the initiation of Antarctic glaciation in the earliest Oligocene, *Global Planet. Change*, *47*, 51–66.

Zachos, J., M. Pagani, L. Sloan, E. Thomas, and K. Billups (2001), Trends, rhythms, and abberations in global climate 65 ma to present, *Science*, *292*, 686–693.

Zachos, J. C., T. M. Quin, and S. Salamy (1996), High resolution (10.000 yr) deep-sea foraminiferal stable isotope records of the earliest Oligocene climate transition, *Paleoceanography*, *11*, 251–266.

M. H. England and M. Huber, Department of Earth and Atmospheric Sciences, Purdue Climate Change Research Center, Purdue University, 550 Stadium Mall Dr., West Lafayette, IN 47907, USA. (m.england@unsw.edu.au; huberm@purdue.edu)

W. P. Sijp, Climate Change Research Centre, University of New South Wales, Sydney, NSW 2052, Australia. (w.sijp@unsw.edu.au)